Article

Not peer-reviewed version

Strategies to Enhance Catalytic Efficiency of ZnO Thin Film under Solar Light Irradiation

Teodora Matei , Gabriel Andrisan , Ioana-Laura Velicu , Georgiana Bulai , Mihai-Alexandru Ciolan , Felicia Gheorghiu , Marius Dobromir , Roxana Strungaru-Jijie , Vasile Tiron *

Posted Date: 14 February 2026

doi: 10.20944/preprints202602.1173.v1

Keywords: ZnO-based thin films; reactive HiPIMS; TVA; piezo-photocatalysis; Ag_2O nanoparticle decoration

 doi:10.20944/preprints202602.1173.v1

Article

Strategies to Enhance Catalytic Efficiency of ZnO Thin Film Under Solar Light Irradiation

Teodora Matei [1], Gabriel Andrisan [1], Ioana-Laura Velicu [1], Georgiana Bulai [2], Mihai Alexandru Ciolan [3], Felicia Gheorghiu [3], Marius Dobromir [3], Roxana Strungaru-Jijie [3] and Vasile Tiron [3,*]

[1] Faculty of Physics, Alexandru Ioan Cuza University of Iasi, Iasi-700506, Romania

[2] Integrated Center of Environmental Science Studies in the North-Eastern Development Region (CERNESIM), Department of Exact and Natural Science, Alexandru Ioan Cuza University of Iasi, Iasi-700506, Romania

[3] Research Center on Advanced Materials and Technologies, Department of Exact and Natural Science, Institute of Interdisciplinary Research, Alexandru Ioan Cuza University of Iasi, Iasi-700506, Romania

* Correspondence: vasile.tiron@uaic.ro

Abstract

Given the increasing environmental degradation, this study investigates advanced ZnO-based materials for the mineralization of toxic compounds through the combined action of photo- and piezocatalysis. Two complementary strategies were employed to enhance catalytic efficiency. First, $ZnO_{1-x}N_x$ thin films were deposited by reactive high-power impulse magnetron sputtering (R-HiPIMS) to reduce the band gap energy. Second, flower-like ZnO nanostructures were synthesized using the pulsed thermionic vacuum arc (TVA) technique to increase the specific surface area. Both systems were further modified by decoration with Ag_2O nanoparticles to improve charge separation. The materials were comprehensively characterized in terms of optical properties (UV–Vis spectroscopy), chemical composition and bonding (XPS), crystalline structure (XRD), surface morphology (FE-SEM), and photo-piezocatalytic performance. Catalytic activity was evaluated via the degradation of methylene blue (MB) under visible light irradiation and mechanical vibrations. Nitrogen incorporation in $ZnO_{1-x}N_x$ thin films led to an increase in photocatalytic efficiency from 20% to 28.7%, while the simultaneous application of light and mechanical stimulation increased efficiency to approximately 50%. Under identical irradiation conditions, Ag_2O-decorated $ZnO/ZnO_{1-x}N_x$ exhibited reaction rate constants up to 65% higher than bare counterparts, attributed to reduced electron–hole recombination. ZnO nanostructures achieved degradation efficiencies of 59%, rising to 88.3% with Ag_2O decoration under solar illumination for 120 min. When combined with mechanical vibrations, after 60 min, the degradation efficiencies reached 93% for ZnO and 98% for Ag_2O/ZnO systems. A photodegradation mechanism of Ag_2O NPs decorated ZnO heterostructures was proposed.

Keywords: ZnO-based thin films; reactive HiPIMS; TVA; piezo-photocatalysis; Ag_2O nanoparticle decoration

1. Introduction

In recent years, environmental pollution has emerged as an increasingly critical issue, with its adverse effects on human health and ecosystem integrity becoming more evident. In response, significant efforts have been directed not only toward identifying alternatives to conventional energy sources but also toward developing effective strategies for the removal or neutralization of hazardous compounds - such as industrial dyes and other toxic substances - that frequently enter wastewater streams through various pathways. As the accumulation of chemical pollutants in aquatic environments continues to rise, conventional wastewater treatment methods - whether physical, chemical, or biological - are proving insufficient. These methods often suffer from limitations such as

 doi:10.20944/preprints202602.1173.v1

low efficacy in removing certain organic pollutants, reduced operational viability, and the potential for generating secondary pollution, thereby necessitating the incorporation of additional treatment stages. Among the most prevalent and persistent pollutants is methylene blue, a representative of the phenothiazine dye class, which is widely utilized in various applications, such in textile, paint, plastic, paper, cosmetic, and pharmaceutical industries. Phenothiazine dyes, including methylene blue, are now recognized for their carcinogenic and mutagenic potential, as well as their toxicity to aquatic organisms and humans.

Solar energy represents a sustainable and promising solution in the global effort to achieve a net-zero environmental impact. Among the various solar-driven technologies, photocatalytic systems offer distinct advantages over traditional photovoltaic cells, particularly in terms of significantly lower production costs, reduced material requirements, and minimal reliance on environmentally harmful manufacturing processes. Photocatalysts are typically derived from readily available and inexpensive substances, such as metal oxides, which can be synthesized as thin films on a variety of substrates - an approach that is both scalable and economically favorable. Furthermore, photocatalytic processes aim for full mineralization of persistent and otherwise non-biodegradable organic pollutants, under ambient pressure and temperature conditions, and without generating secondary toxic by-products.

Following a period during which zinc oxide (ZnO) attracted limited attention and was primarily regarded as a substrate material in electronic applications [1], renewed interest has emerged due to its unique properties. These include high thermal and chemical stability, significant hardness, optical transparency, a high melting point, and elevated electron mobility. Additionally, ZnO is non-toxic and cost-effective, making it an attractive candidate for a wide range of technological and environmental applications. Notably, its high piezoelectric coefficient, alongside its established photocatalytic activity, also renders ZnO suitable for piezocatalytic processes, thereby expanding its utility in advanced catalytic systems.

Despite its many advantageous properties, the practical application of zinc oxide (ZnO) in photocatalysis is hindered by several inherent limitations. One major drawback is its wide band gap (~3.4 eV), which restricts photoactivation to the ultraviolet (UV) region, thereby excluding the more abundant visible light spectrum. Additionally, ZnO exhibits a high recombination rate of photogenerated electron–hole pairs, which significantly reduces its photocatalytic efficiency. Another critical issue is its limited stability during repeated use, primarily due to photocorrosion in aqueous environments under UV irradiation. To address these challenges and enhance ZnO's performance in photocatalytic applications, various research efforts have focused on modification strategies. To enhance the photocatalytic efficiency of zinc oxide (ZnO) and address its intrinsic limitations, multiple research directions have been explored, each targeting one or more strategic modifications. These include the formation of composite materials by coupling ZnO with other materials to improve structural and electronic properties [2,3]. Other strategies involve optimizing the pH of the reaction medium to influence surface charge and pollutant interaction [4,5], as well as doping with elements such as nitrogen [6] or decoration with noble co-catalyst [7,8] to enhance visible-light absorption and reduce charge carrier recombination. Additionally, morphological modifications - such as tuning particle size, shape, or surface area - have been shown to play a significant role in improving photocatalytic activity [9].

An additional approach to improving the catalytic performance of zinc oxide (ZnO) involves leveraging its inherent piezoelectric properties in piezocatalytic processes. In this mechanism, the application of external mechanical stimuli - such as ultrasonic vibrations - induces an internal electric field within the ZnO structure. This field promotes the separation of charge carriers and facilitates the generation of electron–hole pairs, analogous to the photogenerated carriers in photocatalysis. A particularly promising aspect of ZnO lies in its ability to simultaneously exhibit both piezocatalytic and photocatalytic activity. The synergistic effect arising from the coupling of these two mechanisms has been demonstrated to significantly enhance the degradation efficiency of environmental pollutants [10,11].

 doi:10.20944/preprints202602.1173.v1

In this work, the influence of the catalyst's morphology on the piezocatalytic and photocatalytic activity was investigated by synthetizing ZnO in form of smooth thin film and flower-like nanostructured layer.

Among the various techniques employed for thin-film deposition, sputtering is one of the most widely used due to its versatility and reliability. A particularly advanced variation of this method is Reactive High Power Impulse Magnetron Sputtering (R-HiPIMS), which enables superior control over the structural and functional properties of the deposited layers. R-HiPIMS offers several notable advantages, including the formation of high-density, very smooth and uniform thin films onto large surface, with excellent adhesion to the substrate. Moreover, the process achieves relatively high deposition rates, thereby significantly reducing fabrication time. Additionally, R-HiPIMS is characterized by low production costs and the capability to deposit high-quality coatings even on temperature-sensitive substrates. These features, combined with its non-toxic and environmentally friendly nature, make R-HiPIMS a highly attractive and sustainable approach for the fabrication of advanced thin-film materials.

R-HiPIMS operates by sputtering a metallic target within a mixed atmosphere typically composed of an inert gas, such as argon, and a reactive gas. The deposition material is formed through the interaction between target atoms ejected by ion bombardment and reactive gas species present in the plasma. The resulting compound is then deposited onto the substrate. A key advantage of this technique lies in its precise tunability; the composition of the deposited film can be effectively controlled by adjusting the relative flow rates of the inert and reactive gases, thereby enabling the synthesis of stoichiometrically tailored materials.

A common challenge encountered in reactive sputtering processes is the occurrence of hysteresis, which arises from the transition between the metallic and compound (or "poisoned") target modes. This phenomenon can lead to process instability and a significant reduction in the deposition rate. However, the reactive HiPIMS technique offers a distinct advantage by stabilizing the transient regime, thereby enabling the deposition of stoichiometric thin films with improved efficiency. One effective strategy to suppress the hysteresis effect involves minimizing target poisoning during the off-time between pulses. This is achieved by employing short-duration, high-frequency pulses while maintaining a constant average power, thereby reducing the residence time of reactive species on the target surface [12]. Furthermore, this pulsing strategy also contributes to the suppression of arc formation, as the limited charge accumulation time reduces the likelihood of arc initiation on the target surface [13].

In addition, due to its versatility, reactive HiPIMS allows the easy control of chemical composition of compound layer, like oxynitride layer. The mechanism of nitrogen incorporation in metal oxide thin film was presented in previous papers [12,14,15]. Therefore, this deposition technique was also used to change the electronic structure of ZnO thin film by nitrogen doping.

The morphological modifications of ZnO layer - such as particle size, shape, or surface area, can successfully approached by using pulsed Thermionic Vacuum Arc (TVA) deposition technique. The TVA-deposition method is a gas-free plasma source which allows obtaining energetic and intense metal ion flux [16]. The main features and benefits of this physical vapor deposition (PVD) technique consist of highly ionized flux which enables dense, smooth and adhesive films, while during reactive deposition enables process stabilization of the transition regime [17]. In the case of Zn deposition enables synthesis of nanostructured layer, which after thermal oxidation process turns in flower-like ZnO nanostructured layer with very large specific area.

Herein, we report several strategies to enhance catalytic efficiency of ZnO thin film under solar light irradiation, as follow:

- improve crystallinity by thermal annealing;
- electronic structure modification by nitrogen doping;
- morphology modification by nanostructuring;
- surface modification by loading Ag_2O NPs onto ZnO layer;
- piezo-assisted catalysis by combining solar light irradiation with mechanical vibrations

 doi:10.20944/preprints202602.1173.v1

The synthesized layers were examined by different techniques (XPS, XRD, SEM, UV-Vis) and finally used as efficient catalyst for the degradation of Methylene Blue dye under solar light irradiation and solar light irradiation combined with mechanical vibrations. Further, the plausible mechanism for the enhanced activity of Ag_2O NPs decorated ZnO layers has also been proposed.

2. Results and Discussion

2.1. Optical and Chemical Properties of ZnO and $ZnO_{1-x}N_x$ Thin Film Deposited by Reactive HiPIMS.

The optical properties of the zinc oxide and oxynitride thin films deposited on glass substrates were investigated by UV–VIS spectroscopy. Transmittance spectra were recorded over the wavelength range of 370–1100 nm. Figure 1(a) presents the optical transmittance spectra of the thin films deposited at various pulse repetition frequencies, including reference zinc oxide samples deposited at a pulse repetition frequency of 600 Hz.

An initial observation from the transmittance spectra is that, with increasing pulse repetition frequency, the onset of optical transmittance shifts toward higher wavelengths. This redshift suggests a reduction in the optical band gap energy of the $ZnO_{1-x}N_x$ thin films, which is indicative of increased nitrogen incorporation into the lattice. At high repetition frequency, nitrogen may introduce localized acceptor or defect states, and a mixed phases may form.

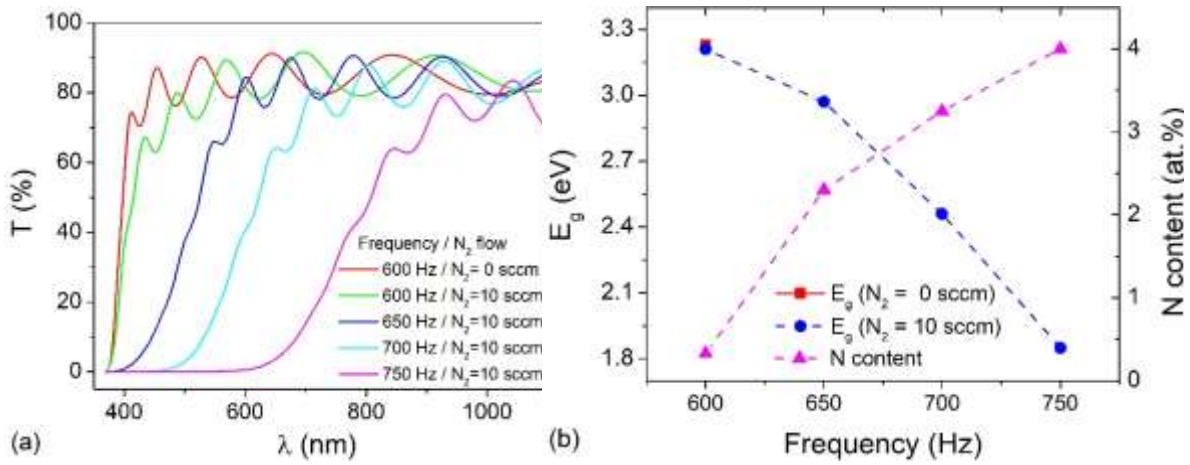

Figure 1. Optical transmittance of ZnO thin films deposited at a pulse repetition frequency of 600 Hz and $ZnO_{1-x}N_x$ thin films deposited at frequencies ranging from 600 to 750 Hz (a) and corresponding band gap values and nitrogen content (b).

To obtain a quantitative estimation of the optical band gap energy, the band gap was determined by extrapolating the linear region of the Tauc plot to its intersection with the photon energy axis. In the Tauc analysis, $(\alpha h\nu)^2$ was plotted as a function of photon energy hν, based on the assumption of a direct allowed transition, as supported by previous studies on the optoelectronic properties of zinc oxynitride [18].

For the zinc oxynitride thin films, an increase in the pulse repetition frequency from 600 to 750 Hz results in a progressive decrease in the optical band gap energy from 3.21 to 1.85 eV. This reduction in band gap energy is attributed primarily to increased nitrogen incorporation in the thin films (Figure 1b). By increasing the repetition frequency, the nitrogen content (estimated from XPS spectra) gradually increases from 0.33 to 4 at.%. Nitrogen introduces intermediate energy states within the band gap, effectively narrowing it. Additionally, the substitution of oxygen by nitrogen leads to the formation of Zn–N bonds, which are less ionic and weaker than Zn–O bonds, further contributing to the observed band gap narrowing [19].

 doi:10.20944/preprints202602.1173.v1

2.2. Structural Analysis of ZnO and $ZnO_{1-x}N_x$ Thin Film

The structural properties of the as-deposited zinc oxynitride ($ZnO_{1-x}N_x$) thin films were investigated by X-ray diffraction (XRD). The resulting diffractograms are presented in Figure 2(a). The red curves represent the diffraction patterns of films deposited in the absence of nitrogen, corresponding to pure zinc oxide (ZnO). In the XRD patterns of zinc oxynitride thin films deposited on glass substrates, the diffraction peaks appear intense, sharp, and well-defined, indicating a high degree of crystallinity and a large crystallite size. The most prominent reflections are observed at approximately 34° and 36°, corresponding to the (002) and (101) crystallographic planes, respectively, of the hexagonal wurtzite phase of ZnO. This suggests that nitrogen atoms have partially substituted oxygen atoms within the ZnO lattice without significantly disrupting the crystalline structure.

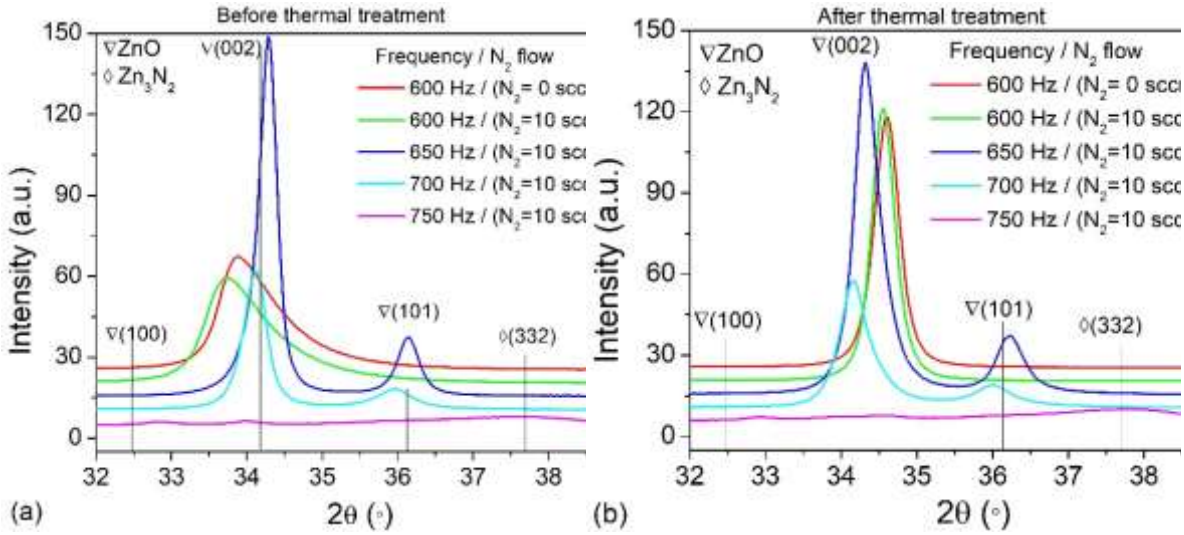

Figure 2. X-ray diffraction (XRD) patterns of ZnO and $ZnO_{1-x}N_x$ thin layers deposited on glass substrates: (a) as-deposited films and (b) after thermal treatment at T = 500 °C for t = 2 h in a nitrogen (N_2) atmosphere.

The thin film deposited at a frequency of 650 Hz exhibits the highest degree of crystallinity, as evidenced by the enhanced peak intensities. This observation supports the hypothesis that a moderate substitution of oxygen atoms with nitrogen, can improve the crystalline quality in the $ZnO_{1-x}N_x$ films. However, at higher deposition frequencies (750 Hz), increased nitrogen incorporation leads to the emergence of a phase mixture, since an additional diffraction peak, attributed to the (332) plane of the Zn_3N_2 phase, appear near 38°. Simultaneously, a notable decrease in the intensity of the ZnO-related peaks is observed, indicating reduced crystallinity. This degradation is likely due to the incorporation of nitrogen atoms in interstitial positions, which act as point defects and disrupt the crystal lattice.

To promote the substitution of oxygen by nitrogen within the $ZnO_{1-x}N_x$ crystal lattice, the thin films deposited on glass substrates were subjected to post-deposition thermal annealing at 500 °C for 2 hours in a nitrogen atmosphere. The X-ray diffraction patterns of the films before and after annealing are presented in Figure 2(b). Following thermal treatment, a noticeable improvement in crystallinity is observed, particularly for ZnO thin film and $ZnO_{1-x}N_x$ thin films deposited at lower pulse repetition frequencies. The diffraction peaks become narrower and more distinct, indicating enhanced crystallite size and reduced lattice disorder. This suggests that thermal annealing facilitates atomic rearrangement and nitrogen incorporation into substitutional sites, thereby improving the structural quality of the $ZnO_{1-x}N_x$ thin films.

2.3. Ag_2O NPs Decoration of ZnO and $ZnO_{1-x}N_x$ Thin Films

The morphologies of the synthesized Ag_2O nanoparticles decorated ZnO and $ZnO_{1-x}N_x$ thin films were examined by scanning electron microscopy (SEM). Figure 3 shows the SEM image of Ag_2O NPs

 doi:10.20944/preprints202602.1173.v1

loaded onto ZnO thin film. The images, taken in "*secondary + back-scattering*" mode, clearly shows that the Ag_2O nanoparticles were successfully loaded on the top surfaces of the ZnO thin film deposited by reactive HiPIMS. Ag_2O NPs are evenly distributed and grown in very high density with irregular shape and sizes (bright dots from Figure 3). The diameters of the Ag_2O nanoparticles were found to be in the range of 30 ÷ 500 nm.

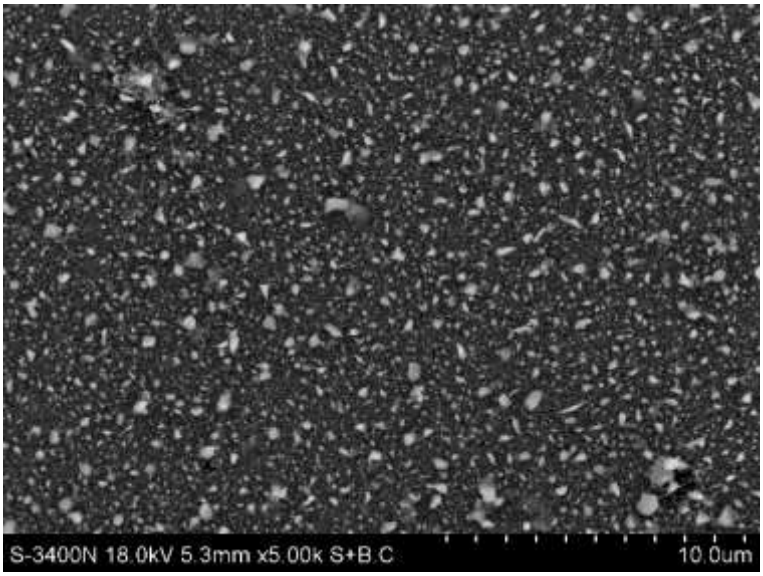

Figure 3. SEM image of Ag_2O NPs loaded onto ZnO thin film.

The oxidation state of Ag_2O/ZnO layer was highlighted by XPS analysis (Figure 4). The XPS spectrum of Zn-2p XPS presents two characteristic peaks which appear at the 1021.6 ± 0.2 eV and 1044.6 ± 0.2 eV, corresponding to the ZnO $2p_{3/2}$ and ZnO $2p_{1/2}$ oxidation state [20]. The O-1s XPS spectrum were deconvoluted into three peaks corresponding to lattice oxide (Zn/Ag-O) at 530 ± 0.2 eV, surface hydroxyl (Zn/Ag-OH) at 531.5 ± 0.2 eV and loosely bound oxygen, such as absorbed O^{2-} or adsorbed H_2O at 533.2 ± 0.2 eV [21]. In the case of Ag-3d, the characteristic peaks are located at 367.4 ± 0.2 eV and 373.4 ± 0.2 eV, corresponding to the Ag_2O $3d_{5/2}$ and Ag_2O $3d_{3/2}$ oxidation state [22].

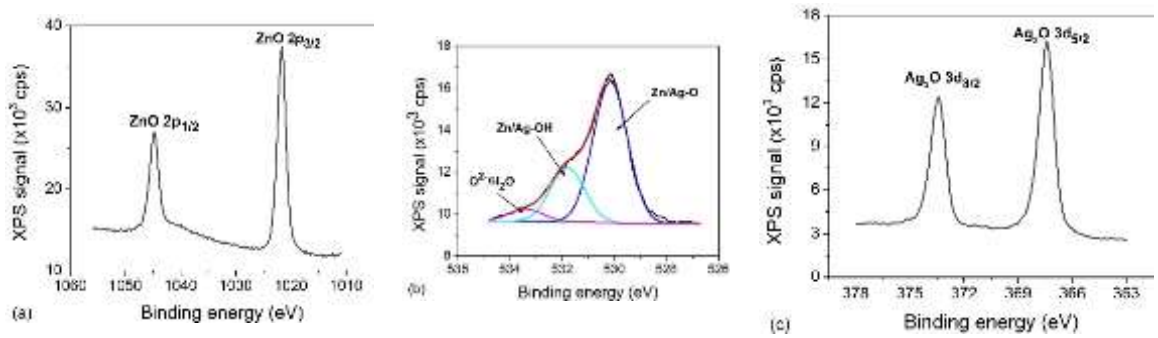

Figure 4. High resolution XPS spectra of Zn-2p (a), O-1s (b) and Ag-3d (c) recorded from ZnO thin film deposited at pulsing frequency of 600 Hz, after cleaning using Ar ion sputtering.

2.4. Characterization of Nanostructured Zn and ZnO Thin Films Deposited by Pulsed TVA

The structural properties of the synthesized nanostructured Zn and ZnO thin film were investigated by X-ray diffraction. Figure 5 shows the X-ray-diffraction patterns for as-deposited Zn coatings synthesized by PTVA and for the corresponding thermal-annealed coating (ZnO). The diffraction patterns of the as-deposited Zn coating confirm the presence of Zn phase (according to PDF card no. 04-0831), with the main diffraction peaks positioned at 36.34°, 39.08° and 43.3°, 54.42°,

 doi:10.20944/preprints202602.1173.v1

70.2°, 70.74° and 77.08° which are assigned to the (002), (100), (101), (1002), (103), (110) and (004) planes of pure Zn, respectively. The multitude of diffraction peaks indicates a polycrystalline hexagonal structure of Zn layer.

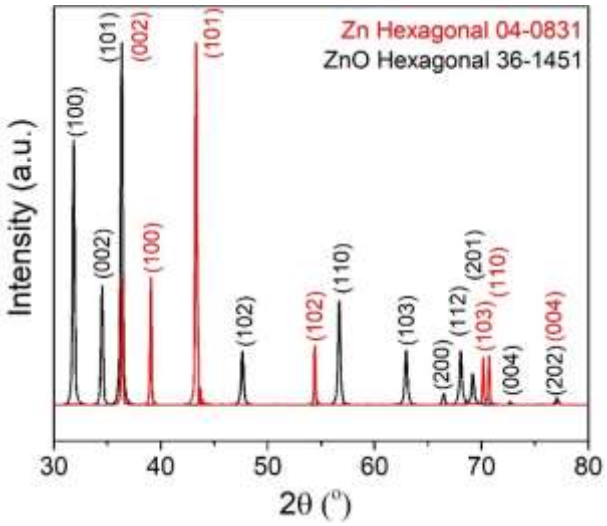

Figure 5. X-ray diffraction (XRD) patterns of nanostructured Zn and ZnO layers deposited on silicon substrates. Each pattern was normalized to the maximum intensity.

After thermal annealing in oxygen atmosphere, only peaks corresponding to the wurtzite ZnO phase (according to PDF card no. 36-1451), are found in the diffraction pattern. All the peaks corresponding to as-deposited Zn coating disappeared, indicating a complete oxidation process of the Zn coatings. In addition, strong diffraction peaks (> 10^4 cps) indicate good crystalline structure. The average grain size, estimated from the diffraction peaks' width using Scherrer's equation [23], is 60 ± 5 nm in the case of the as-deposited Zn coating and 38.5 ± 1.2 nm in the case of the corresponding thermal-annealed coating (ZnO).

2.5. Ag_2O NPs Decoration of Nanostructured ZnO Thin Films Deposited by Pulsed TVA

The presence of Ag_2O NPs onto nanostructured ZnO layer is highlighted by the SEM analysis. Figure 6 illustrates the morphologies of as-deposited Zn layer, nanostructured ZnO layer obtained after thermal-annealing in oxygen atmosphere, and Ag_2O NPs loaded onto nanostructured ZnO layer.

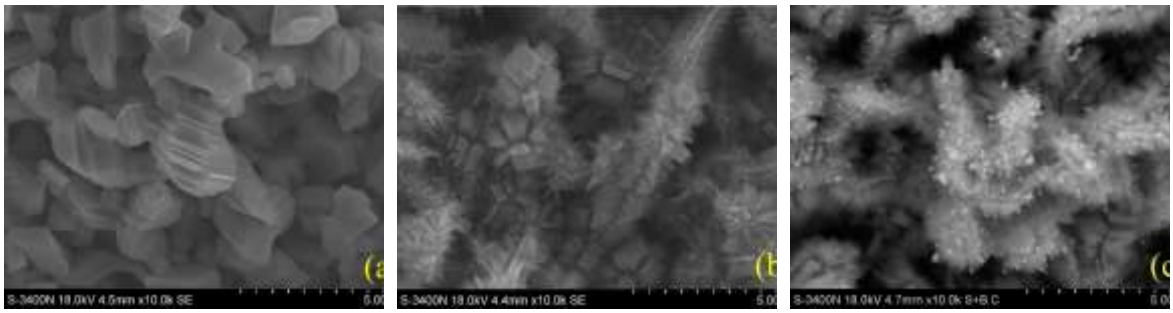

Figure 6. SEM image of nanostructured Zn thin film (a), nanostructured ZnO thin film (b) and Ag_2O NPs loaded onto ZnO nanostructured thin film (c).

The Zn coating deposited by PTVA onto Si substrate exhibits an aspect of nanostructured layer consisting of individual structures with irregular and regular shapes (hexagonal structures made by stacks of nanosheets) and different sizes (Figure 6a). After thermal annealing in oxygen atmosphere, the resulting ZnO layer exhibits brush-like and flower-like surface morphology with high density and very fine nanorods (Figure 6b). It seems that the nanorods grow normal to the facets of

 doi:10.20944/preprints202602.1173.v1

hexagonal-shaped nanostructures. Figure 6(c) shows that Ag_2O NPs with spherical shape and irregular sizes are uniform loaded onto nanostructured ZnO layer. To better highlight the presence of Ag_2O NPs the SEM images was captured in "*secondary + back-scattering*" mode. The typical sizes of the nanoparticles attached on the nanorods were in the range of 40-100 nm.

2.6. Catalytic Performance

2.6.1. ZnO and $ZnO_{1-x}N_x$ Thin Films Deposited onto Glass Substrate by Reactive HiPIMS

The catalytic performance of ZnO and $ZnO_{1-x}N_x$ thin films deposited onto glass substrate was evaluated through their piezo-photocatalytic degradation of MB dye. The experimental data acquisition protocol involved collecting measurements at 15-minute intervals during the first hour, followed by 30-minute intervals during the second hour.

Figure 7 illustrates the temporal evolution of the MB concentration and the corresponding pseudo-first-order kinetic analysis, *-ln(C/C0)*, for zinc oxynitride thin films deposited on glass substrates and subsequently subjected to thermal treatment in a nitrogen atmosphere. Data were acquired under three conditions: exposure to simulated solar illumination, and combined exposure to illumination and mechanical vibrations, and Ag_2O decorated zinc oxynitride thin films under simulated solar illumination. To establish a benchmark for evaluating the photo-piezocatalytic activity of zinc oxynitride thin films, the absorption spectra of methylene blue solutions were recorded in the absence of the catalyst. These control experiments enabled the construction of reference degradation curves, represented in black in graph and labeled as "*Blank*". In the case of measurements conducted under illumination conditions only, an approximately linear increase in degradation efficiency is observed with increasing pulse repetition frequency. Specifically, the efficiency increases from 20.0% for the $ZnO_{1-x}N_x$ thin film deposited at 600 Hz to 28.7% for the film deposited at 750 Hz.

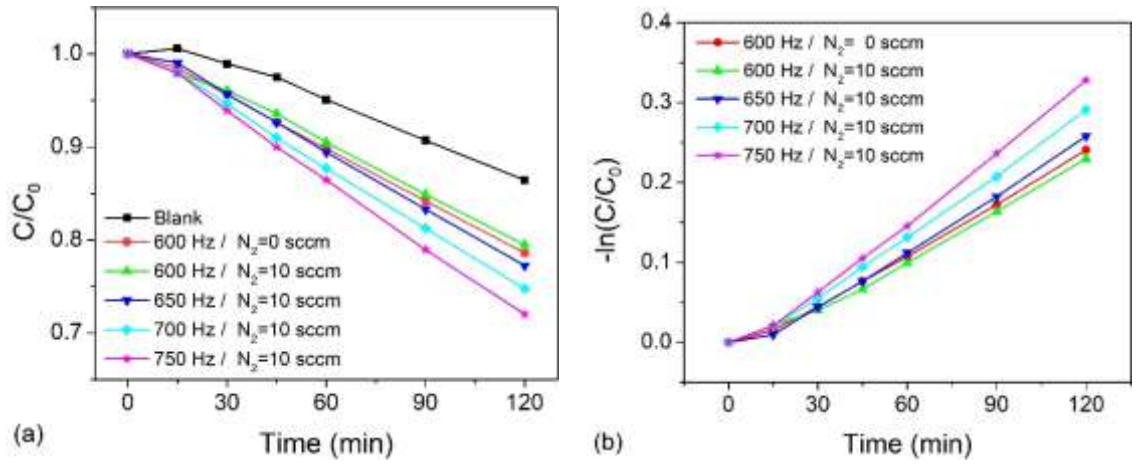

Figure 7. Temporal evolution of the methylene blue solution concentration (a) and corresponding pseudo-first-order kinetic analysis (b) for ZnO and $ZnO_{1-x}N_x$ thin films under simulated solar illumination.

The reaction constant values (k), determined using a pseudo-first-order kinetic model (Figure 7b), highlights better the photocatalytic efficiency of each sample. Figure 8 illustrates the reaction constant values for MB photo-decomposition by ZnO and $ZnO_{1-x}N_x$ thin films under simulated solar illumination. By increasing the repetition frequency from 600 to 750 Hz, the reaction constant gradually increases from 2×10^{-3} min^{-1} to 2.8×10^{-3} min^{-1}. This enhancement in photocatalytic performance is attributed to the higher nitrogen incorporation at elevated deposition frequencies, which leads to a narrowing of the band gap (Figure 1b). As a result, light absorption within the visible spectrum becomes more efficient, thereby promoting the generation of electron–hole pairs that actively participate in the dye degradation reactions.

 doi:10.20944/preprints202602.1173.v1

A similar trend is observed in the case of measurements performed under combined solar illumination and mechanical vibration conditions, where the reaction constant increases from 2.67×10^{-3} min^{-1} for the $ZnO_{1-x}N_x$ thin film deposited at 600 Hz to 3.76×10^{-3} min^{-1} for the film deposited at 750 Hz. By combining solar illumination with mechanical vibration, the degradation rate increases for all samples, with gain values ranging from 35% to 50%.

However, this increase does not follow the linear behavior observed under illumination-only conditions. Notably, the thin film deposited at 650 Hz exhibits the most pronounced increase, with a reaction constant which is nearly equivalent to the maximum value recorded. Although this sample exhibits a slightly higher band gap compared to those deposited at higher frequencies, its superior crystallinity and preferential growth along the crystallographic plane associated with enhanced piezoelectric properties result in significantly improved piezocatalytic activity. This compensates for the relatively lower photocatalytic contribution, leading to an overall degradation efficiency comparable to the highest observed value.

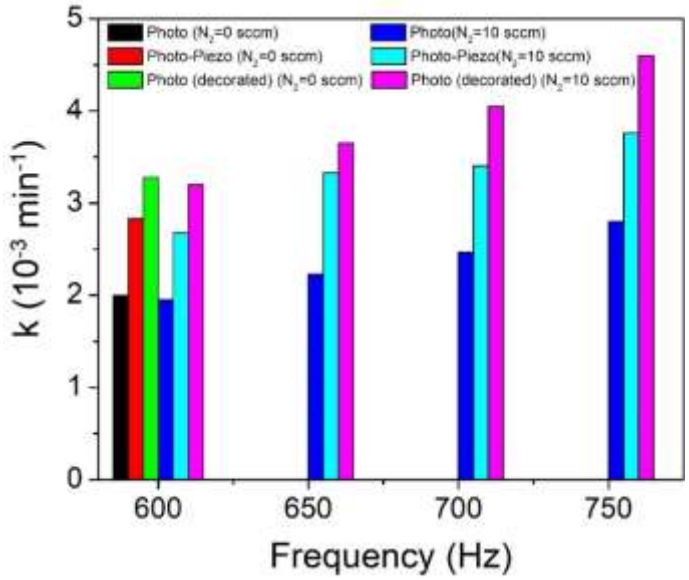

Figure 8. Reaction constant values for MB decomposition by ZnO, $ZnO_{1-x}N_x$, Ag_2O/ZnO and Ag_2O/ $ZnO_{1-x}N_x$ thin films under simulated solar illumination and combined solar light illumination and mechanical vibrations.

By combining solar light illumination with mechanical vibrations, the catalytic efficiency increases due to occurrence of local piezoelectric field which allow a better transport and separation of photo-generated charges. However, the increase in catalytic efficiency is limited by the fact that the piezo-active material is fixed on a rigid and dielectric support (glass substrate) that limits the transmission of vibrations and prevents the transport of charge carriers toward one side of the film.

In the case of Ag_2O/ZnO and Ag_2O/ $ZnO_{1-x}N_x$ thin films, the photocatalytic efficiency under simulated solar illumination is even higher than piezo-photocatalytic efficiency of bare ZnO and $ZnO_{1-x}N_x$ thin films. The reaction constant values for photo-decomposition of MB by Ag_2O/ZnO and Ag_2O/ $ZnO_{1-x}N_x$ thin films are 65% higher than in the case of bare ZnO and $ZnO_{1-x}N_x$ photocatalyst. The pronounced increase in the photocatalytic efficiency of Ag_2O-decorated ZnO thin film could be ascribed to less electron-hole recombination. A plausible mechanism for the enhanced activity of Ag_2O NPs decorated ZnO layers is proposed in the next subsection.

2.6.2. ZnO Nanostructured Thin Films Deposited onto Silicon Substrate by Pulsed TVA

The photocatalytic degradation efficiency of MB dye in the absence or presence of nanostructured ZnO and Ag_2O/ZnO catalysts under simulated solar light irradiation and combined illumination with mechanical vibrations is shown in Figure 9(a). The result indicates that under simulated solar light irradiation and combined illumination with mechanical vibrations for 2 h, the

 doi:10.20944/preprints202602.1173.v1

MB solution is quite stable, reaching a degradation rate of 13.5% and 19%, respectively. Under simulated solar light irradiation, about 59% of dye removal takes place in the presence of the nanostructured ZnO, and 88.3% in the presence of the Ag_2O/ZnO photocatalysts. The catalytic efficiency of both nanostructured layer is more pronounced under combined simulated solar light irradiation and mechanical vibrations. After 60 min *ca.* 93% of MB dye is removed by ZnO catalyst, and approximatively 98% by the Ag_2O/ZnO catalyst. The contributions of loaded Ag_2O NPs and mechanical vibration (piezoelectric effect) to catalytic efficiency of nanostructured ZnO layer are better highlighted the reaction constant (k) plotted in the Figure 9(b). By adding Ag_2O NPs and mechanical vibration the degradation rate (k) of nanostructured ZnO layer is improved by 8.6 times. Moreover, under identical conditions (illumination time and light intensity), as compared to the ZnO thin film deposited by reactive HiPIMS, the degradation rate is enhanced by 32.3 times.

The outstanding piezo-photocatalytic activity of the Ag_2O/ZnO layers is due to a collective contribution of favorable factors, such as:

- high degree of crystallinity of nanostructured ZnO layer (improve the transport and lifetime of charge carriers);
- nanostructured morphology (enhance catalytic efficiency due to very large specific area and efficient charge transport);
- surface modification by loading Ag_2O NPs onto ZnO layer (enhance visible light activity due to narrow energy band-gap of Ag_2O and reduced charge recombination rate);
- piezo-assisted catalysis by combining solar light irradiation with mechanical vibrations (enhance catalytic activity due to efficient separation and transport of photo-generated charge).

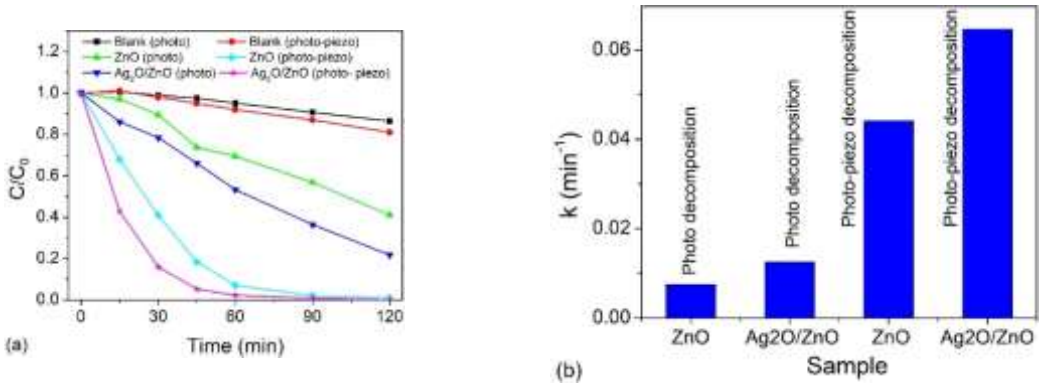

Figure 9. Temporal evolution of the methylene blue solution concentration (a) and reaction constant values for MB decomposition (b) for ZnO and Ag_2O/ZnO nanostructured thin films under simulated solar illumination and combined illumination with mechanical vibrations.

2.7. Photodegradation Mechanism of Ag_2O NPs Decorated ZnO Heterostructures

The enhanced photocatalytic activity of decorated ZnO thin films and nanostructured layer could be attributed to the presence of Ag_2O NPs on their surface, which together form a hetero-junction. It is well known that the formation of hetero-junction could improve the photocatalytic activity of dual semiconductors due to better separation of photogenerated electron-hole pairs. The separation of electrons and holes arises from the fact that the photoexcitation of an electron from valence band (VB) of one semiconductor results in an electron transfer to the lower conduction band (CB) of the second semiconductor [24]. In the case of ZnO thin film catalyst, the conduction band (CB) potentials can be estimated by the following empirical equation [25]:

$$E_{CB} = X - E_e - 0.5E_g \quad (3)$$

where E_{CB} is the CB edge potential, X is the electronegativity of the semiconductor, E_e is the energy of free electrons, while E_g is the band-gap energy of semiconductor. The absolute electronegativity X of ZnO is 5.89 eV, while the energy of free electrons (E_e) is 4.5 eV *vs.* NHE (normal hydrogen electrode). Considering that, in this work, the E_g is 3.21 eV for ZnO thin film (estimated from Tauc

 doi:10.20944/preprints202602.1173.v1

plot), the calculated energy levels of CB and VB are -0.215 eV and 2.995 eV, respectively. A quite similar E_g value was reported by Ma et al. [10] for ZnO nanorods. For Ag_2O NPs it is difficult to estimate E_g from Tauc plot, that's why the values of valence and conduction band potentials were taken from Ref. [26], as 1.38 eV and -0.27 eV, respectively. When a heterojunction is formed between ZnO and Ag_2O NPs, due to their potential difference in bands energy, the holes from the VB of ZnO would migrate to the VB of Ag_2O, while the electrons from the CB of Ag_2O would migrate to the CB of ZnO (Figure 10), leading to a better charge carrier separation, and consequently, to a reduced recombination rate.

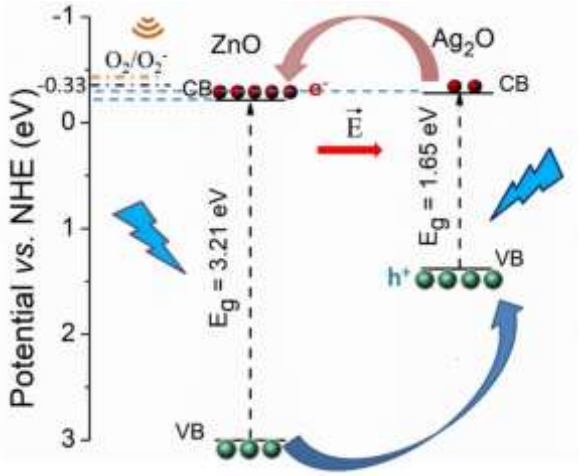

Figure 10. Schematic illustration for the calculated energy level diagram of Ag_2O/ZnO hetero-junction.

The separation and transfer of electrons and holes through the semiconductor' bands lead to a build-in electric field at the Ag_2O/ZnO interface, which acts like a driven force and facilitates the migration and separation of holes and electrons to the catalyst's surface, enhancing its photocatalytic activity. Therefore, Ag_2O NPs loaded onto ZnO surface act as an inhibitor of electron – hole pairs recombination in the catalyst by and promoting the transfer of interfacial electron. Moreover, under simulated solar light irradiation, due to its narrower band gap energy (1.65 eV), Ag_2O NPs catalyst acts as visible light sensitized which injects more electrons into the conduction band of ZnO. However, the CB edges of both Ag_2O (-0.27 eV) and ZnO (-0.215 eV) are less negative than redox potential of O_2/O_2^- (-0.33 eV) and it can't reduce O_2 molecule to superoxide radical O_2^-. On the other hand, the VB edge of ZnO (2.995 eV) is more positive than the oxidation potential of OH^-/•OH (1.99 eV) and it can produce •HO free radicals by the oxidation of hydroxyl ions OH^-, which in turn are generated by CB holes interaction with adsorbed H_2O molecules (oxidation potential of H_2O is 2.73 eV). Consequently, the expected photodegradation pathway of MB under simulated solar light is mainly due to photogenerated holes which can directly decompose the MB molecules *via* highly oxidizing •OH free radicals.

Under combined action of simulated solar light irradiation and mechanical vibrations, the high piezo-potential induced by mechanical stress in ZnO nanostructures can lead to energy band bending [27], which in turn facilitate the electrons from CB of ZnO to participate to O_2/O_2^- reduction reactions. Outstanding piezopotential value of 0.3 V was reported for ZnO nanowire [28]. In this work, in the absence of mechanical vibration, the difference between CB position (-0.215 V) of ZnO and redox potential for the reduction of oxygen (-0.33 V) is very small, only 0.115 V. Therefore, it is expected that the large strain induced by the mechanical vibration to be sufficient to shift the CB position to redox potential level favorable for the generation of O_2^- radicals by reduction of O_2.

Therefore, the high quantum efficiency of Ag_2O/ZnO heterostructures under the combined action of simulated solar light irradiation and mechanical vibrations may be attributed to the synergistic effect between Ag_2O NPs, which prolong the lifetime of the excited electron – hole pairs,

 doi:10.20944/preprints202602.1173.v1

and to the piezo-potential induced by mechanical stress in ZnO nanostructures, which causes a band bending, thereby enabling O_2/O_2^- reduction reactions.

The present work could shed light on the understanding of catalysis mechanisms and contribute to the development of efficient photocatalysts for the environmental remediation by fully utilizing light and vibration energy.

3. Materials and Methods

3.1. Synthesis of Zinc Oxynitride Thin Films by Reactive HiPIMS

The thin film deposition system employed for the fabrication of zinc oxynitride layers comprises a stainless-steel vacuum chamber capable of reaching a base pressure of 10^{-4} Pa. This vacuum level is achieved using a combination of a mechanical pump (Dry Scroll) and a turbo-molecular pump (Agilent Technologies).

To ensure the presence of a sufficient density of charge carriers within the deposition chamber prior to the application of high voltage pulses, a high-voltage pulse generator is employed to establish a pre-ionized pulsed discharge regime. The implementation of a pre-ionized regime facilitates a rapid rise in discharge current intensity, offering significant advantages over conventional HiPIMS techniques, particularly in terms of plasma stability and deposition efficiency [29].

Thin films of zinc oxynitride were deposited onto glass substrates using a zinc target with a purity of 99.95%, a diameter of 50 mm, and a thickness of 3 mm. The substrates (glass slide with square shape, 25mm × 25mm size) were electrically grounded by clamping to a grounded substrate holder and were not subjected to intentional heating during deposition. Prior to deposition, a 5-minute pre-sputtering step was performed with the substrates shielded by a screen to remove any surface contaminants from the target and to establish a stable sputtering regime.

Thin film depositions were conducted under a balanced magnetic field configuration, with a fixed target-to-substrate distance of 8 cm. The deposition chamber pressure was maintained at 3 Pa, and the deposition duration was approximately 30 minutes for all samples. To optimize the growth of zinc oxynitride films, a reactive gas mixture consisting of high-purity (99.999%) argon, nitrogen, and oxygen was employed, with respective mass flow rates of 10 sccm, 10 sccm, and 2 sccm. High-power monopolar electrical pulses, characterized by a pulse duration of 10 μs, a constant amplitude of -800 V, and pulse frequency varied between 600 and 750 Hz, were applied to Zn target to obtain zinc oxynitride thin film with different amount of nitrogen. It should be noted that at high repetition frequency a mixed phase may form.

3.2. Synthesis of Zinc Oxide Nanostructured Layers by Pulsed Thermionic Vacuum Arc

TVA-deposition method, operated in pulsed mode, was used to synthesize Zn nanostructured layers, which were subsequently annealed at 800℃ in oxygen atmosphere to obtain the nanostructured ZnO coatings. An extensive description of TVA operating principle and experimental setup is given by Tiron *et al.* in a recent paper [30]. Zn layers were deposited onto silicon substrates (square shape, 25mm × 25mm) fixed on an electrically grounded substrate holder, axially positioned at 16 cm above the anode. TVA discharge parameters were set to voltage amplitude U = 900 V, peak current I = 4 A, pulse duration τ = 200 μs and repetition frequency ν = 500 Hz, and filament current of 28 A. The average discharge power during PTVA operation was 265 W. The deposition time was set to 3 min, and the substrates were unintentionally heated during deposition process. The layer's thickness was 3 μm and was monitored during deposition process using a Quartz Crystal Microbalance. The as-deposited Zn coatings were then annealed at temperature up to 800℃ under an oxygen atmosphere at pressure 1 Pa to obtain ZnO nanostructures. The annealing process was carried out in a high vacuum stainless-steel chamber using a programmable heater system with a heating/cooling rate of 6.5℃/min.

3.3. Ag_2O NPs Decoration

 doi:10.20944/preprints202602.1173.v1

The decoration of the HiPIMS deposited ZnO and $ZnO_{1-x}N_x$ thin films and TVA deposited ZnO nanostructured layers with silver oxide nanoparticles (Ag_2O NPs) was performed according to the protocol described by Al-Gharibi *et al.* [31]. The ZnO based thin films deposited on glass or silicon substrate were immersed in a solution of silver nitrate ($AgNO_3$, S6506-25G) with concentrations of 0.5 mM, solution prepared from a mixture of water-ethanol (volumetric rate 4:1), and exposed to radiation emitted by a UV lamp (8 W, λ =253.7 nm) for 5 minutes. Subsequently, samples were rinsed with ultrapure water and subjected to a heat treatment at 300℃ for one hour, under ambient conditions (B510, Model L3/11 B510, L-034K1LN1, Nabertherm).

3.4. Characterization Techniques

The optical properties of the zinc oxynitride thin films deposited onto glass substrates were characterized by UV–VIS spectroscopy. Transmission spectra were acquired by a double-beam UV-1901 recording spectrophotometer (Beijing Puxi General Instrument Co., Ltd., Beijing, China) in the spectral range of 370 – 1100 nm, using bare glass substrate as the baseline. Based on the recorded transmission spectra, the optical band gap energy of the thin films was determined using Tauc plots, derived from the absorption coefficient as a function of photon energy.

The chemical composition and structure of the HiPIMS deposited zinc oxynitride thin films and Ag_2O/ZnO thin films deposited by TVA were investigated by XPS (PHI 5000 VersaProbe XPS system from ULVAC PHI Inc., monochromatic Al Kα X-ray source, beam diameter of 100 μm²). The binding energy values have been calibrated using as reference the carbon C-1s peak (284.6 eV). High resolution spectrum of the O-1s peak was fitted using a non-linear least-squares method (Multi Pak 8.2 C software) with a Gaussian–Lorentzian function (prior to each fit, the background was subtracted using the Shirley method).

The structural properties of the thin films, including crystallographic orientation and phase identification, were analyzed by X-ray diffraction (XRD) using a Shimadzu LabX XRD-6000 diffractometer. Measurements were performed with CuKα radiation (λ = 1.54 Å) in the Bragg–Brentano θ–2θ geometry. Diffractograms were recorded over a 2θ range of 20°–80°, with a scanning speed of 1°/min and a step size of 0.02°.

The morphology of bare $ZnO_{1-x}N_x$ and ZnO thin films deposited by reactive HiPIMS and pulsed TVA, and Ag_2O NPs decorated ZnO thin films was investigated by using a field emission scanning electron microscope (Hitachi S-3400N).

The photo-piezocatalytic activity of the thin films was evaluated by monitoring the degradation efficiency of a methylene blue (MB) aqueous solution (03978, Sigma-Aldrich, Darmstadt, Germany) under simultaneous visible light irradiation and mechanical vibration. Visible light was provided by a solar simulator (Oriel, model LCS-100) equipped with a 100 W Xenon arc lamp, delivering a maximum incident light intensity of 100 mW/cm². Mechanical vibrations were applied using an FALC LBS 2 ultrasonic bath operating at a frequency of 40 kHz and a power of 70 W. During the experiments, the solution temperature was maintained at 25 °C to ensure consistent reaction conditions.

Prior to initiating the photo-piezocatalytic experiments, all samples were immersed in the MB solution (15 mg/L, 15 mL) for 30 minutes in the dark to establish adsorption–desorption equilibrium. The photo-piezocatalytic activity was then assessed over a 120 min period, during which the degradation of the dye was monitored every 15 min intervals, during the first hour, followed by 30 min intervals during the second hour. Absorbance measurements were performed at a wavelength of 664 nm using a V-10 Plus spectrophotometer, with the solution placed in a quartz cuvette (10 mm path length). The degradation efficiency (η) and reaction rate constant (k) were calculated using the following equations:

$$\eta\ (\%) = (C_0 - C_t)/C_0 \times 100 \quad (1)$$

$$\ln (C_0/C_t) = -kt \quad (2)$$

 doi:10.20944/preprints202602.1173.v1

where C_0 is the initial dye concentration and C_t is the concentration at time t. Control experiments, performed under identical illumination and mechanical vibration conditions but in the absence of thin film catalysts, were also conducted to account for photolysis or other non-catalytic effects.

The concentration of the MB solution during the degradation experiments was determined using a previously established calibration curve. This curve was constructed from a series of standard MB solutions with concentrations ranging from 0.1 to 15 mg/L. The corresponding UV–VIS absorption spectra were recorded over the wavelength range of 190–750 nm. The calibration curve (y = 0,0846 + 0,1274x) was obtained by plotting the absorbance at the maximum absorption wavelength (λ_{max} = 664 nm) against the known concentrations.

4. Conclusions

This study focused on the synthesis and comprehensive evaluation of zinc oxynitride thin films deposited by reactive high-power impulse magnetron sputtering (R-HiPIMS) and ZnO nanostructures obtained via the pulsed thermionic vacuum arc (TVA) techniques, as well as on the enhancement of their properties through surface decoration with silver oxide nanoparticles. The catalytic performance of all investigated systems was assessed through the degradation of methylene blue under simulated solar light irradiation, mechanical vibrations, and their combined action, enabling the evaluation of both photocatalytic and piezocatalytic contributions.

For zinc oxynitride thin films, the samples were deposited at pulse repetition frequencies between 600 and 750 Hz on glass substrates. Optical and structural analyses revealed that increasing the pulse repetition frequency leads to higher nitrogen incorporation, resulting in a progressive reduction of the band gap energy. Correspondingly, the photocatalytic degradation efficiency increased from 20% to 28.7% with increasing pulse repetition frequency, consistent with enhanced visible-light absorption. The simultaneous application of mechanical vibrations further increased the overall degradation efficiency to approximately 50%. The highest efficiencies were achieved for silver-decorated thin films, highlighting the critical role of suppressed electron–hole recombination in improving catalytic performance.

ZnO nanostructures deposited by pulsed TVA demonstrated significantly enhanced catalytic activity due to their high crystallinity and large specific surface area associated with their morphology. Photocatalytic efficiencies of 59% were obtained for bare ZnO nanostructures, increasing to 88.3% upon silver oxide nanoparticle decoration, attributed to band gap narrowing and reduced charge carrier recombination. When visible light irradiation was combined with mechanical stimulation, degradation efficiencies after one hour reached 93% for ZnO and 98% for Ag-decorated ZnO nanostructures.

The high quantum efficiency observed in Ag_2O/ZnO heterostructures under simulated solar light and mechanical vibrations likely results from the combined effect of Ag_2O nanoparticles, which extend the lifespan of excited electron-hole pairs, and the piezoelectric potential generated by mechanical stress in ZnO nanostructures, which causes energy band bending, facilitating O_2/O_2^- reduction reactions.

Overall, the obtained data indicate that structural engineering through nitrogen incorporation, morphological control via nanostructuring, and surface modification with silver nanoparticles constitute effective strategies for enhancing photo-piezocatalytic performance, offering a cost-effective and environmentally friendly approach for the mineralization of organic pollutants.

Author Contributions: Conceptualization, T.M. and V.T.; methodology, R.J-S, V.T.; validation, T.M., R.J-S and V.T.; formal analysis, T.M., G.A.; G.B.; M.A.C.; F.G.; M.D.; and R.J-S; investigation, T.M.; R.J-S.; and V.T.; resources, G.B.; M.A.C.; M.D.; and R.J-S.; data curation, R.J-S.; and V.T.; writing—original draft preparation, T.M.; I-L. V.; and V.T.; writing—review and editing, R.J-S.; I-L. V.; and V.T.; visualization, I-L. V.; supervision, V.T.; project administration, V.T.; funding acquisition, T.M.; and G.A. All authors have read and agreed to the published version of the manuscript.

Funding: The authors acknowledge the support provided by the project "*Integrated interdisciplinary system for the implementation of sustainable development activities in the North-East Region of Romania – SIDNER*" (Cod SMIS: 337821), project co-funded through the Regional Program North-East 2021–2027, Investment priority: PRNE_P1, A more competitive, more innovative region, Call: RDI activities in collaboration with SMEs and investments in public RDI organizations and universities, oriented towards the needs identified in the regional entrepreneurial discovery process, Project call number: PR/NE/2024/P1/RSO1.1/1/2 – RDI INFRASTRUCTURES. R. S.-J. acknowledges the support provided by the Ministry of Education and Research, CNCS - UEFISCDI, project number PN-IV-P2-2.1-TE-2023-0258, within PNCDI IV program.

Data Availability Statement: Data is contained within the article or supplementary material.

Conflicts of Interest: The authors declare no conflicts of interest.

References

1. Janotti, A.; Van de Walle, C.G. Fundamentals of zinc oxide as a semiconductor. Rep. Prog. Phys. 2009, 72, 126501. https://doi.org/10.1088/0034-4885/72/12/126501
2. Sun, W.; Li, J.; Mele, G.; Zhang, Z.; Zhang, F. Enhanced photocatalytic degradation of rhodamine B by surface modification of ZnO with copper (II) porphyrin under both UV–vis and visible light irradiation. J. Mol. Catal. A Chem. 2013, 366, 84–91. https://doi.org/10.1016/j.molcata.2012.09.010
3. Campagnolo, L.; Lauciello, S.; Athanassiou, A.; Fragouli, D. Au/ZnO hybrid nanostructures on electrospun polymeric mats for improved photocatalytic degradation of organic pollutants. Water 2019, 11, 1787. https://doi.org/10.3390/w11091787
4. Han, J.; Liu, Y.; Singhal, N.; Wang, L.; Gao, W. Comparative photocatalytic degradation of estrone in water by ZnO and TiO2 under artificial UVA and solar irradiation. Chem. Eng. J. 2012, 213, 150–162. https://doi.org/10.1016/j.cej.2012.09.066
5. Puri, N.; Gupta, A. Water remediation using titanium and zinc oxide nanomaterials through disinfection and photocatalysis process: A review. Environ. Res. 2023, 227, 115786. https://doi.org/10.1016/j.envres.2023.115786
6. Shinde, S.S.; Bhosale, C.H.; Rajpure, K.Y. Photocatalytic degradation of toluene using sprayed N-doped ZnO thin films in aqueous suspension. J. Photochem. Photobiol. B 2012, 113, 70–77.
7. Han, Z.; Ren, L.; Cui, Z.; Chen, C.; Pan, H.; Chen, J. Ag/ZnO flower heterostructures as a visible-light driven photocatalyst via surface plasmon resonance. Appl. Catal. B Environ. 2012, 126, 298–305. https://doi.org/10.1016/j.apcatb.2012.07.002
8. Al-Mamun, R.; Islam, S.; Hossain, R.; Kader, S.; Islam, S.; Khan, Z.H. A novel and highly efficient Ag and GO co-synthesized ZnO nano photocatalyst for methylene blue dye degradation under UV irradiation. Environ. Nanotechnol. Monit. Manag. 2021, 16, 100495. https://doi.org/10.1016/j.enmm.2021.100495
9. Nosrati, R.; Olad, A.; Maramifar, R. Degradation of ampicillin antibiotic in aqueous solution by ZnO/polyaniline nanocomposite as photocatalyst under sunlight irradiation. Environ. Sci. Pollut. Res. 2012, 19, 2291–2299. https://doi.org/10.1007/s11356-011-0736-5
10. Xue, X.; et al. Piezo-potential enhanced photocatalytic degradation of organic dye using ZnO nanowires. Nano Energy 2015, 13, 414–422. https://doi.org/10.1016/j.nanoen.2015.02.029
11. Ma, J.; et al. High efficiency bi-harvesting light/vibration energy using piezoelectric zinc oxide nanorods for dye decomposition. Nano Energy 2019, 62, 376–383. https://doi.org/10.1016/j.nanoen.2019.05.058
12. Tiron, V.; Sirghi, L. Tuning the band gap and nitrogen content of ZnOxNy thin films deposited by reactive HiPIMS. Surf. Coat. Technol. 2015, 282, 103–106. https://doi.org/10.1016/j.surfcoat.2015.10.017
13. Tiron, V.; Velicu, I.-L.; Matei, T.; Cristea, D.; Cunha, L.; Stoian, G. Ultra-short pulse HiPIMS: A strategy to suppress arcing during reactive deposition of SiO2 thin films with enhanced mechanical and optical properties. Coatings 2020, 10, 633. https://doi.org/10.3390/coatings10070633
14. Demeter, A.; Samoila, F.; Tiron, V.; Stanescu, D.; Magnan, H.; Straticiuc, M.; Burducea, I.; Sirghi, L. Visible-light photocatalytic activity of TiOxNy thin films obtained by reactive multi-pulse high power impulse magnetron sputtering. Surf. Coat. Technol. 2017, 324, 614–619. https://doi.org/10.1016/j.surfcoat.2016.10.011

15. Matei, T.; Tiron, V.; Jijie, R.; Bulai, G.; Velicu, I.-L.; Cristea, D.; Craciun, V. Band-gap engineering of zirconia by nitrogen doping in reactive HiPIMS: A step forward in developing innovative technologies for photocatalysts synthesis. Front. Chem. 2023, 11, 1239964. https://doi.org/10.3389/fchem.2023.1239964
16. Musa, G.S.; Ehrich, H.; Schuhmann, J. Pure metal vapor plasma source with controlled energy of ions. IEEE Trans. Plasma Sci. 1997, 25, 386–391.
17. Tiron, V.; Porosnicu, C.; Dinca, P.; Velicu, I.-L.; Cristea, D.; Munteanu, D.; Révész, Á.; Stoian, G.; Lungu, C.P. Beryllium thin films deposited by thermionic vacuum arc for nuclear applications. Appl. Surf. Sci. 2019, 481, 327–336. https://doi.org/10.1016/j.apsusc.2019.03.096
18. Khan, Z. Optical and structural properties of ZnO thin films fabricated by sol-gel method. Mater. Sci. Appl. 2011, 2, 340–345. https://doi.org/10.4236/msa.2011.25044
19. Futsuhara, M.; Yoshioka, K.; Takai, O. Optical properties of zinc oxynitride thin films. Thin Solid Films 1998, 317, 322–325. https://doi.org/10.1016/S0040-6090(97)00646-9
20. Moulder, J.F.; Stickle, W.F.; Sobol, P.E.; Bomben, K.D. Handbook of X-ray Photoelectron Spectroscopy; ULVAC-PHI: Japan/USA, 1995.
21. Shirsath, S.E.; Liu, X.; Yasukawa, Y.; Li, S.; Morisako, A. Switching of magnetic easy-axis using crystal orientation for large perpendicular coercivity in CoFe2O4 thin film; Sci. Rep. 2016, 6, 30074. https://doi.org/10.1038/srep30074
22. Zhao, W.; Zhang, J.; Zhu, F.; Mu, F.; Zhang, L.; Dai, B.; Xu, J.; Zhua, A.; Sun, C.; Leung, D.Y.C. Study the photocatalytic mechanism of the novel Ag/p-Ag2O/n-BiVO4 plasmonic photocatalyst for the simultaneous removal of BPA and chromium (VI). Chem. Eng. J. 2019, 361, 1352–1362. https://doi.org/10.1016/j.cej.2018.12.181
23. Waseda, Y.; Matsubara, E.; Shinoda, K. X-ray Diffraction Crystallography: Introduction, Examples and Solved Problems; Springer Science & Business Media: Berlin/Heidelberg, Germany, 2011.
24. Li, S.; Lin, Y.-H.; Zhang, B.-P.; Li, J.-F.; Nan, C.-W. BiFeO3/TiO2 core-shell structured nanocomposites as visible-active photocatalysts and their optical response mechanism. J. Appl. Phys. 2009, 105, 054310. https://doi.org/10.1063/1.3091286
25. Butler, M.A.; Ginley, D.S. Prediction of Flatband Potentials at Semiconductor–Electrolyte Interfaces from Atomic Electronegativities. J. Electrochem. Soc. 1978, 125, 228–232. https://doi.org/10.1149/1.2131419
26. Sugiura, E.; Furukawa, M.; Tateishi, I.; Katsumata, H.; Kaneco, S. Development of Ag/Ag2O/ZnO photocatalyst and their photocatalytic activity towards dibutyl phthalate decomposition in water. J. Air Waste Manag. Assoc. 2022, 72, 1137–1152. https://doi.org/10.1080/10962247.2022.2071358
27. Chimupala, Y.; Phromma, C.; Yimklan, S.; Semakul, N.; Ruankham, P. Dye wastewater treatment enabled by piezo-enhanced photocatalysis of single component ZnO nanoparticles. RSC Adv. 2020, 10, 28567–28575. https://doi.org/10.1039/D0RA04746E
28. Gao, Y.; Wang, Z.L. Equilibrium potential of free charge carriers in a bent piezoelectric semiconductive nanowire. Nano Lett. 2009, 9, 1103–1110. https://doi.org/10.1021/nl803547f
29. Velicu, I.-L.; Tiron, V.; Popa, G. Dynamics of the fast HiPIMS discharge during FINEMET-type films deposition. Surf. Coat. Technol. 2014, 250, 57–64. https://doi.org/10.1016/j.surfcoat.2014.03.015
30. Tiron, V.; Ciolan, M.A.; Bulai, G.; Mihalache, G.; Lipsa, F.D.; Jijie, R. Efficient removal of methylene blue and ciprofloxacin from aqueous solution using flower-like nanostructured ZnO coating under UV irradiation. Nanomaterials 2022, 12, 2193. https://doi.org/10.3390/nano12132193
31. Al-Gharibi, M.A.; Kyaw, H.H.; Al-Sabahi, J.N.; Myint, M.T.Z.; Al-Sharji, Z.A.; Al-Abri, M.Z. Silver nanoparticles decorated zinc oxide nanorods supported catalyst for photocatalytic degradation of paracetamol. Mater. Sci. Semicond. Process. 2021, 134, 105994. https://doi.org/10.1016/j.mssp.2021.105994